


X-ray holography of skyrmionic cocoons in aperiodic magnetic multilayersM. Grelier¹,* F. Godel¹, A. Vecchiola¹, S. Collin, K. Bouzehouane¹, V. Cros¹, and N. Reyren¹†
*Unité Mixte de Physique, CNRS, Thales, Université Paris-Saclay, 91767, Palaiseau, France*R. Battistelli¹*Helmholtz-Zentrum Berlin für Materialien und Energie, 14109 Berlin, Germany*H. Popescu, C. Léveill e, and N. Jaouen¹*Synchrotron SOLEIL, L'Orme des Merisiers, 91192, Gif-sur-Yvette, France*F. B uttner¹*Helmholtz-Zentrum Berlin f ur Materialien und Energie, 14109 Berlin, Germany
and Augsburg University, 86159, Augsburg, Germany* (Received 26 January 2023; accepted 5 June 2023; published 22 June 2023)

The development and characterization of three-dimensional (3D) topological magnetic textures has become an important topic in modern magnetism both for fundamental and technological perspectives. Among the novel 3D spin textures, skyrmionic cocoons have been successfully stabilized in magnetic multilayers having a variable thickness of the ferromagnet in the vertical direction of the stack. These ellipsoidal 3D magnetic textures remain vertically confined in a fraction of the total thickness, whereas, coexisting with fully columnar skyrmions. Here, we use x-ray holography with about 15-nm lateral resolution to investigate how their properties depend on the field and temperature. We observe circular objects with different amplitude of contrast, which evidences the presence of different 3D objects located in various vertical parts of the multilayer. Moreover, whereas, sweeping an out-of-plane magnetic field, we witness an attractive interaction between cocoons located at various heights, mainly due to the stray field, which impacts their horizontal positionings. The x-ray holography measurements also allow to determine the size of the cocoons at remanence, which at room temperature, possess diameters close to 100 nm on average. Combining this transmission technique with magnetic force microscopy and micromagnetic simulations gives a precise insight into the 3D distribution of the magnetization, which demonstrates the 3D nature of skyrmionic cocoons.

DOI: [10.1103/PhysRevB.107.L220405](https://doi.org/10.1103/PhysRevB.107.L220405)

Introduction. Magnetic topological textures have been identified as promising information bits for the development of next-generation spintronic devices especially in terms of stability and energy consumption. A pioneer example of such objects remains the magnetic skyrmion [1–4], a two-dimensional (2D) whirl of the magnetization that is in most cases stabilized by the Dzyaloshinskii-Moriya interaction (DMI), arising from broken inversion symmetry and large spin-orbit coupling. Skyrmions can be observed in chiral magnets or in magnetic multilayers where they acquire a vertical tubular shape, however, in some cases with a hybrid chirality over the z direction [5,6]. Despite the potential of skyrmions and other 2D topological textures, a new interest has arisen for more complex quasiparticles that display variations over the thickness, i.e., three-dimensional (3D) objects [7,8]. The added dimensionality can lead to more intricate magnetic distribution, which allows the range of perspective applications to be broadened [9,10]. As a consequence, an ever-growing

set of 3D solitons is already developing. For instance, in noncentrosymmetric crystals, magnetic bobbars that correspond to half tubular skyrmions ending with a Bloch point buried inside the ferromagnetic film have been recently observed [11–14] as well as the topologically trivial dipole strings [15,16] in bulk compounds. In magnetic multilayered thin films, truncated skyrmions [17,18], skyrmion braids [19], or even hopfions [20,21] have been reported. A recent newcomer is the skyrmionic cocoon [22], so named due to its peculiar ellipsoidal shape. We recently stabilized such cocoons in aperiodic multilayers with a complex distribution of the magnetic interactions, making use of the tunability of such structures. Skyrmionic cocoons only reside in a fraction of the multilayers, and this vertical confinement can be tuned either by optimizing the multilayer architecture or by using an external magnetic field. Interestingly, they can coexist with more usual textures, such as columnar skyrmions, an attractive feature both for the explanation of fundamental phase transitions between different topological states [23] and for potential applications, such as racetrack memories based on different types of 3D textures [12].

In this paper, we report a nonperturbative observation of skyrmionic cocoons as well as their field-dependent behavior

*matthieu.grelier@cnsr-thales.fr

†Corresponding author: nicolas.reyren@cnsr-thales.fr

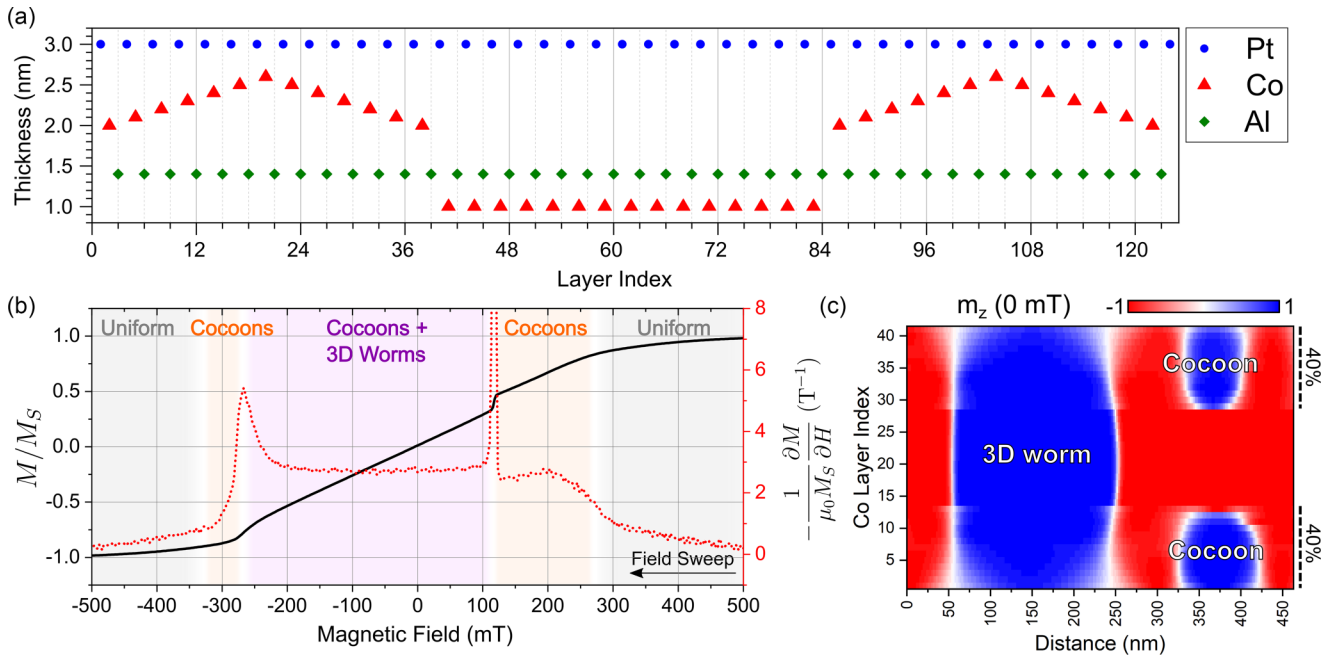


FIG. 1. Properties of the magnetic multilayer with a variable ferromagnetic layer thickness. (a) Thickness distribution of the Pt/Co/Al trilayers for each layer. (b) The out-of-plane component of the magnetization normalized by M_S measured via AGFM along with its derivative. The background colors identify the various expected magnetic phases expected from the derivative transitions. (c) Cut of m_z over the thickness showing the simultaneous presence of skyrmionic cocoons along with columnar textures at remanence. The indicated percentage values relate to the proportion of the total magnetization.

measured via x-ray holography with extended reference by autocorrelation linear differential operator (HERALDO) [24] along with x-ray Fourier transform holography (FTH) experiments [25]. HERALDO and FTH are lensless high-resolution transmission techniques that record the hologram resulting from the interferences between an object hole and a reference aperture, a slit for the former and a hole for the latter. Those create a reference wave that encodes the phase so that a simple Fourier transform directly allows to recover a real-space image of the actual magnetic configuration of the sample. The spatial resolution is typically limited by the size of the reference aperture as well as by the numerical aperture of the setup. To improve the contrast and the resolution, one can additionally make use of phase retrieval algorithms [26] for the image reconstruction. The experiments have been performed on the COMET [27] end station of the SEXTANTS beamline located at the SOLEIL synchrotron using a transmission setup to measure first the circularly left (CL) polarization followed by the circularly right (CR) one at the Co L_3 edge (778.8 eV). The vertical component of the magnetization averaged over the material thickness can then be extracted from the difference between the real-space reconstructions of the two polarization images, which informs about the thickness extent of the 3D magnetization textures. As holography is a transmission technique, it allows to probe the averaged magnetization distribution, contrarily to more accessible techniques, such as magnetic force microscopy (MFM), which is more surface sensitive. The comprehensive field evolution study of skyrmionic cocoons, including the holography measurements along with MFM and micromagnetic simulations, allows to better characterize these new 3D textures.

Results. Multilayers hosting skyrmionic cocoons. We recently showed with MFM that skyrmionic cocoons can be stabilized in magnetic multilayers displaying variable thicknesses of the ferromagnetic films thanks to the induced inhomogeneous distribution of the magnetic interactions [22]. The architecture considered in the HERALDO study is detailed in Fig. 1(a), notably showing the thickness evolution of the successive trilayers Pt/Co/Al (layer number is shown in the horizontal axis). This schematic evidences three distinguishable parts: the top and bottom ones in which the Co thickness varies from layer to layer that we later on, call the gradient parts, and the middle ones (between layer number 38 and 84) where the Co thickness is fixed at 1 nm to have a strong perpendicular magnetic anisotropy (PMA). The sample imaged with FTH was slightly modified as the thickness of the Pt layers in the top gradient have been altered (see Methods for the precise structures). The multilayers have been grown by sputtering deposition on the top side of a Si_3N_4 membrane with a backside covered with a 1.1- μm -thick gold mask layer that was milled away with focused ion beam, yielding for HERALDO (respectively, FTH) a 2- μm diameter (respectively, 800 nm) round object hole. In Fig. 1(b), the alternating gradient force microscopy (AGFM) curve displays the magnetization M normalized by the saturation magnetization M_S for an out-of-plane (OOP) magnetic field sweeping from positive to negative. In conjugation with micromagnetic simulations performed with MUMAX3 [28], it is possible to identify the various magnetic phases hosted by the multilayer based on the transitions in the signal derivative, following our method described in Ref. [22]. Starting at the high positive field, the magnetization points uniformly along the field direction.

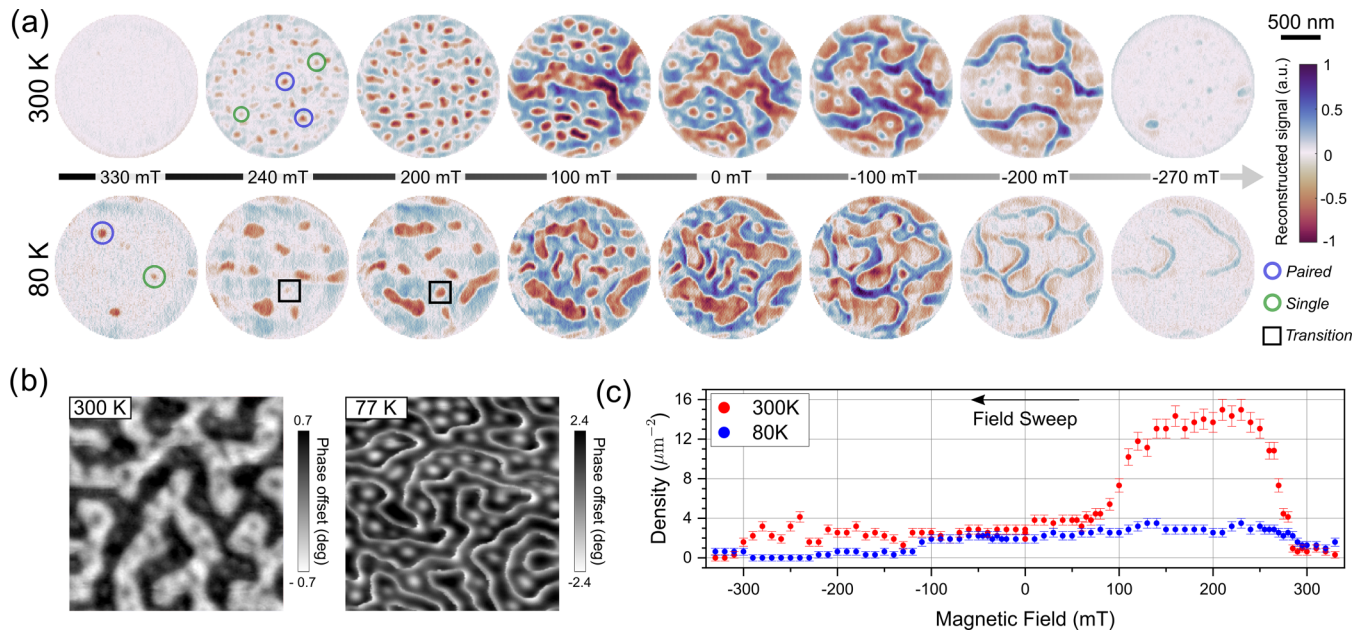


FIG. 2. HERALDO imaging performed with a 2- μm object hole. (a) Field dependency measured at 300 (top row) and 80 K (bottom row). The colored shapes put forward examples of paired or single cocoons cocoons as well as transitions between the two states. (b) MFM images ($3 \times 3 \mu\text{m}^2$) at remanence at room temperature (left) and 77 K (right). The length scale is common to (a). (c) Evolution of the density of isolated objects based on HERALDO measurements.

Upon the decrease in the field, around 275 mT, skyrmionic cocoons begin to nucleate in the gradient parts of the structure whereas the middle layers are still pointing up. At 125 mT, a jump is measured in the magnetization, which corresponds to the formation of domains that extend over the whole thickness of the multilayer, which we will call 3D worms or 3D stripes. At remanence, a coexistence is observable between those 3D worms and skyrmionic cocoons that are only present in the top and bottom outer parts with the Co gradients [see Fig. 1(c)]. Decreasing more, the magnetic field can transform the 3D worms into columnar skyrmions and ultimately provokes the disappearance of textures in the strong PMA layers, leaving again only cocoons behind (between -260 and -325 mT) that will eventually be annihilated near -325 mT. In Fig. 1(c), a vertical cut of the vertical component of the magnetization (m_z) obtained with micromagnetic simulations illustrates the spatial vertical extent of each of the textures at remanence, which can evolve significantly with the magnetic field.

Temperature and field dependency of skyrmionic cocoons.

To investigate these magnetic textures, HERALDO measurements have been performed at 300 and 80 K, whereas, sweeping an OOP magnetic field from positive saturation to negative. As predicted numerically [22], the spin textures present in the sample under focus will significantly evolve, whereas, varying the magnetic field. Representative maps of the vertical component of the magnetization in the object hole are presented in Fig. 2(a) (the full field dependency is available in the Supplemental Material [29]). At 300 K (top row), starting from near saturation at 330 mT, skyrmionic cocoons have nucleated when lowering the field as shown with the image at 240 mT. As the signal scales with m_z averaged over the thickness, the existence of two different contrasts is indicative of the existence of various objects. The weaker contrast corresponds to a single cocoon, located either in the

top or the bottom gradient layers, whereas, the stronger one is linked to paired cocoons, one on top of the other. Based on the hysteresis measurements, when decreasing the field from positive saturation the middle layers should only accommodate domains for fields lower than 125 mT, which, thus, prohibits the existence of full columnar skyrmions above that field. Those observations thus confirm the presence of different 3D textures. Then, at 100 mT, large stripes begin to propagate into the field of view, corresponding to 3D worms extending over the full thickness, which are still surrounded by paired cocoons. The measurement is not accurate enough to allow to differentiate between paired cocoons and 3D worms as it only represents a 20% variation in the signal but the results can be correlated with concomitant MFM and simulations. At remanence, a mixed state of 3D worms and paired cocoons is observed. Upon the decrease in the magnetic field, the stripes of up magnetization get narrower and paired cocoons emerge in their stead. Finally, at -270 mT, we can observe a few sparse skyrmionic cocoons along with a few columnar skyrmions, near the bottom left for instance. It should be noted that the use of a beam stop to block the specular signal results in the loss of low-frequency information, which hinders quantitative analysis. This also explains why the two saturation states (with only a low-frequency signal) exhibit similar backgrounds, even though they should have opposite signs.

At 80 K [bottom row in Fig. 2(a)], the overall evolution is similar, however a few discrepancies can be noted. First, a field of 330 mT is not sufficient to saturate the magnetization. Notably, at positive fields, the cocoons appear to be larger and fewer in number than at room temperature. A transition between a single cocoon and a paired one is visible between the second and third frames as indicated by the significant change in contrast in the black squares. According to magnetotransport measurements (see the Supplemental Material [29]), the

TABLE I. Magnetic parameters measured at different temperatures.

Temperature (K)	K_u (MJ/m ³)	M_S (MA/m)
80	0.93 ± 0.03	1.26 ± 0.02
300	0.82 ± 0.03	1.22 ± 0.02

nucleation in the strong PMA layer should happen near 30 mT. Thus, at remanence, a few 3D worms are visible as well as some elongated pairs of cocoons, which correspond to the smaller objects. Other remanent states are shown in Fig. S1 (see the Supplemental Material [29]), showing an image at low temperature more similar to its 300 K counterpart. Finally, decreasing the magnetic field below zero does not induce the nucleation of skyrmionic cocoons: the 3D worms simply shrink and disappear.

To complement the holography measurements, MFM measurements have been performed without an external field at room temperature and at 77 K [Fig. 2(b)]. As the latter is more sensitive to the magnetization close to the surface, it can be correlated with the holography results that relate to the average magnetization of all the magnetic layers. At 300 K, the same characteristic pattern of stripes with smaller white dots in between is obtained. As the signal originates from the divergence of the stray field, the weakly contrasted dots have to correspond to skyrmionic cocoons present in the top gradient of the structure and not to fully columnar skyrmions [22]. Thus, it follows that the isolated objects detected near remanence in HERALDO are paired cocoons. At low temperature, the phase signal mainly detects the domain walls, which could be due to the magnetization of the tip flipping or due to an increase in the sample's anisotropy [30]. However, it still displays two types of structures and appears similar to its high-temperature counterparts. This can be expected as no magnetic field was applied during or after the cool down so that the magnetic state was left undisturbed, i.e., frozen in, and might be metastable. In Fig. 2(c), the field dependency of the density of isolated objects is plotted for the two temperatures. At 300 K, it is coherent with the phase diagram predicted in Fig. 1(b) as the cocoons start to nucleate near 280 mT, hence, the increase in the density, and the nucleation of domains in the PMA layers near 125 mT lower the number of cocoons. It, thus, drops from nearly 15 objects per μm^2 to oscillate around 3 objects per μm^2 below 50 mT. The density at the high negative field depends on the way the 3D worms disappears so variations are expected depending on the magnetic history. At 80 K, the density does not exceed 4 objects per μm^2 over the whole field range. The observed differences can be attributed to the evolution of the magnetic parameters with the temperature. The anisotropy was determined through transport measurements (the Supplemental Material [29]), whereas, the saturation magnetization was retrieved with superconducting quantum interference device (SQUID) (see Table I).

As the skyrmionic cocoons can be stabilized with this increased anisotropy and magnetization saturation, it confirms that they can be observed over a large range of magnetic parameters and, thus, inside many multilayers architectures. Micromagnetic simulations were also performed using the low-temperature parameters to verify their reliability and the

field behavior was found consistent with the measurements (see the Supplemental Material [29]).

Thanks to the large field of view (2 μm), the object hole accommodates many different features, which have been fitted, when possible, with a two-dimensional rotated Gaussian model for every field (see Methods). For potential applications, it is important to have isolated objects as small as possible, which, thus, justify the necessity to characterize the cocoon size distribution based on those holography measurements. An example with the coexistence of isolated and paired cocoons is studied in Fig. 3(a), at 300 K and 240 mT as shown in the inset. The average full width at half maximum (FWHM) and the amplitude of the Gaussian for each object are displayed in the histograms, and the right panel shows a typical fit that was performed on a cocoon. The average sizes are scattered on a large range, starting as small as 50 nm up to 130-nm diameter. Similarly, the amplitudes span different values, the lowest corresponds to single cocoons, whereas, the highest are more likely to be associated with paired cocoons. Then, for each magnetic field, the quartiles of the average FWHM were extracted and the results are presented in Fig. 3(b) at 300 and 80 K where the first and third quartiles serve as error bars to frame the median value, whereas, the color encodes the density. The characteristic diameter at low temperature displays a stronger dispersion, reaching sizes above 200 nm, whereas, at room temperature, it mostly stays below 130 nm. In both cases, we can note the almost linear increase in the size when decreasing the field from positive saturation.

Magnetic phase transitions and interactions. As an alternative measurement, the second sample with a slightly different Pt distribution was probed using FTH through an 800-nm object hole. The recorded holograms have been reconstructed making use of phase retrieval algorithms to improve the contrast and resolution (see Methods for details). For a better visual display, a bilinear interpolation has been performed on the reconstructions, increasing the number of pixels by a factor of 1.25. In Fig. 4(a), FTH reconstructed real-space images of the object hole are displayed at different OOP fields starting from a demagnetized state, prepared with a field tilted at 45° with respect to the sample normal. At first, only two dark red 3D stripes are visible. As the field increases, they get narrower, and some cocoons with a weaker contrast, start to appear at 260 mT. At 320 mT, the stripes have transformed into columnar skyrmions, still accompanied by single cocoons. Furthermore, the images at 342 and 348 mT put forward the transition between a columnar skyrmion and two vertically aligned cocoons (as highlighted with the pink circles), which have a stronger contrast than the single cocoon also visible in those frames. Although it was not possible to differentiate the two states at remanence, the difference at high field is significant enough to classify them. This is also supported by the numerical prediction of this type of transition [22].

In Fig. 4(b), we start from near saturation with a few skyrmionic cocoons and lower the magnetic field, which allows the nucleation of more skyrmionic cocoons as shown with the image measured at 327 mT. The density continues to rise, as expected from the previous study, until the cocoons begin to interact. Looking closer at the transitions between 306 and 280 mT, the “merging” of two pairs of skyrmionic

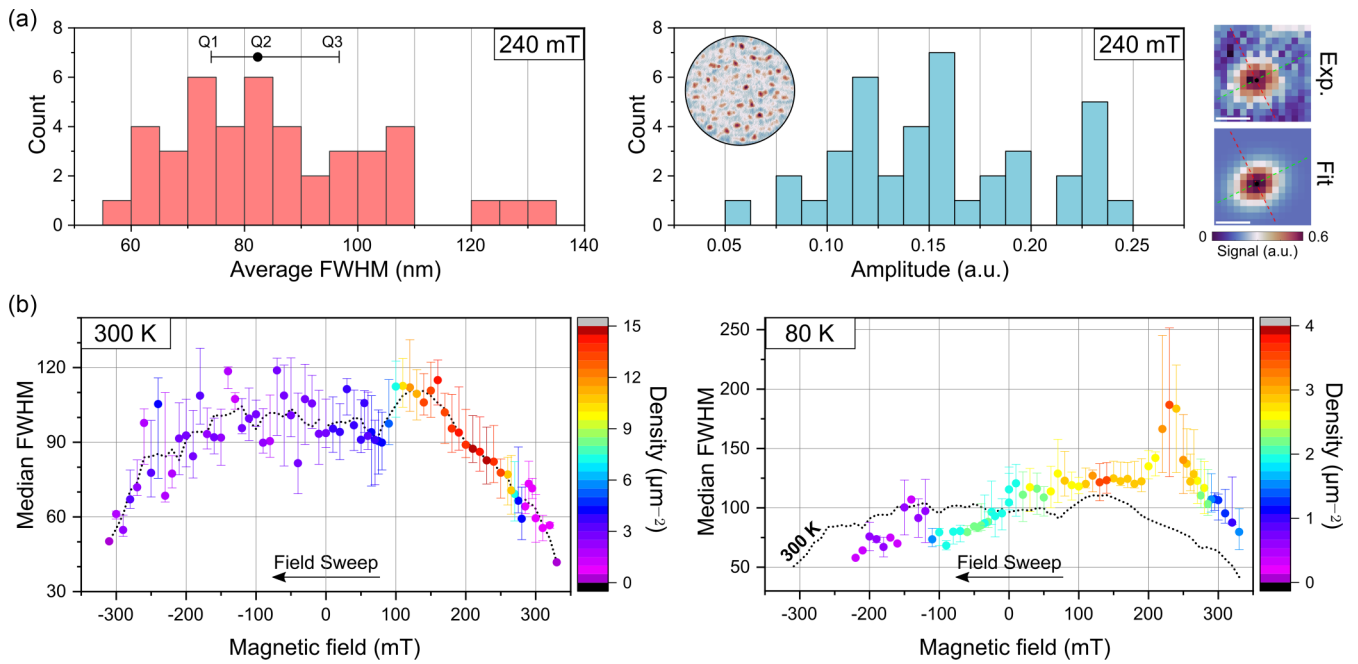


FIG. 3. Size study of the isolated objects observed with HERALDO based on two-dimensional Gaussian fits. (a) Size and amplitude distribution at 240 mT. The images at the right display an example of experimental data along with the corresponding fit. The two dotted lines, respectively, correspond to each of the FWHMs, which are then averaged for each object to yield the size histogram. The white scale in both images is 60-nm long and pixels are $15 \times 15 \text{ nm}^2$. The inset image shows the magnetic state in the 2- μm object hole with a reduced color scale. (b) Field evolution of the median FWHM (Q2) along with the color-coded density at 300 and 80 K. The error bars correspond to the first (Q1) and third quartile (Q3) of the average FWHM as illustrated in (a).

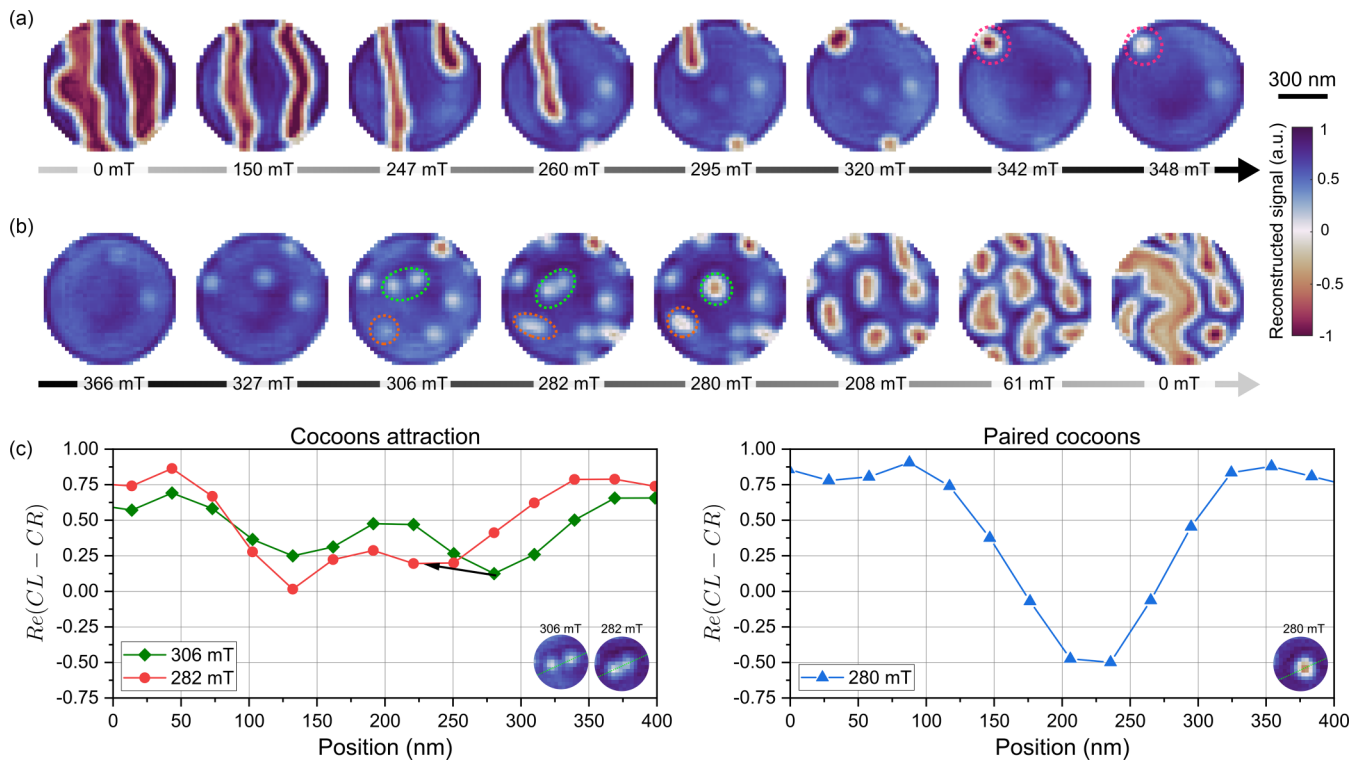


FIG. 4. FTH imaging performed with a 800-nm object hole. Dependency with (a) increasing and (b) decreasing magnetic field. The colored ellipses follow the same textures over different fields to highlight the associated transitions. (c) Study of the transition between two isolated cocoons. The black arrow indicates the relative motion of the cocoons between the two successive fields. The position of the line cut has been changed between the two graphs, but the inset shows the same sample area (a circle of a 200-nm radius).

cocoons can be observed as evidenced by the colored ellipses. Indeed, the cocoons appear to be attracted to one another, implying that one resides in the bottom gradient and the other one in the top one. This transition, which places them one on top of the other, allows to reduce the dipolar interaction, thus, reaching a minimum of energy. The absence of more transitions of this kind at higher fields is most likely due to pinning of the cocoons caused by inhomogeneities in the magnetic interactions associated with the material's grains formed during growth (see the Supplemental Material [29] and Refs. [31–33]). Only when the field is lowered, the cocoons expand and increase their dipolar energy until it is sufficiently strong to overcome the pinning, thus, allowing their alignment. As the field decreases further (for instance at 208 mT), additional aligned cocoons appear and become more elongated. At remanence, we observe again a 3D worm surrounded by paired cocoons as supported by MFM and micromagnetic simulations.

In Fig. 4(c), profiles are shown at different fields to illustrate the transition between the single cocoon state to the double one, evidencing the associated change in contrast. Interestingly, at first, only one of the cocoons is moving towards the other (see black arrow on the left graph), which suggests that the latter is pinned. However, once merged, the two aligned cocoons have slightly moved away from their previous position, a motion likely due to interactions with the other magnetic objects. This peculiar attractive interaction as well as the change in contrast confirms the 3D nature of the skyrmionic cocoons.

Conclusion. The x-ray holography experiments demonstrate the presence of various 3D magnetic textures in aperiodic multilayers. Additionally, it allows an in-depth study of the field-dependent behavior of skyrmionic cocoons, which evidenced complex interactions between them, mostly governed by the dipolar interaction. Those effects are strong enough to move the skyrmionic cocoons by a typical distance of the order of 50 nm so that they can align themselves to end up one atop the other. It also puts forward the various magnetic phases that undergoes the magnetization under an external field as well as the associated phase transitions, which were captured by those measurements. The temperature study highlights a large range of stability for the skyrmionic cocoons even though their size and density may vary. The holography precision limit regarding the contrast does not systematically allow us to distinguish between fully columnar textures and two vertically aligned cocoons as it only represents a difference of 20% of the total magnetization. However, the input from MFM and micromagnetic simulations allows to confidently determine their actual nature. This Letter, thus, establishes that 3D skyrmionic cocoons can reside in different vertical positions of the multilayer, i.e., in the bottom and the top gradients, which could serve as a first basis towards the development of a 3D memory device.

Acknowledgments. Financial support from FLAG-ERA SographMEM (ANR-15-GRFL), from ANR under Grants No. ANR-17-CE24-0025 (TOPSKY), No. ANR-20-CE42-0012 (MEDYNA), and No. ANR-22 DFG (TOPO3D) and as part of the “Investissements d’Avenir” program SPiCY

(ANR-10-LABX-0035). R.B. and F.B. acknowledge funding from the Helmholtz Young Investigator Group Program. We would like to thank M. Bonnet and M. Vallet for access and operation of the FIB to prepare the HERALDO sample.

Methods. Sample preparation and characterization. The samples have been grown on thermally oxidized silicon substrates using magnetron sputtering at room temperature. A seed layer of 5-nm Ta is typically used, and 3-nm Pt capping is deposited to protect from oxidation. In details, the HERALDO sample corresponds to $\text{Ta5|Pt3|}(\text{Co}[2.0:0.1:2.5]|(\text{Al1.4|Pt3}) (\text{Co}[2.6:0.1:2.0]|(\text{Al1.4|Pt3}))(\text{Co1.0|Al1.4|Pt3}) \times 15|(\text{Co}[2.0:0.1:2.5]|(\text{Al1.4|Pt3}) (\text{Co}[2.6:0.1:2.0]|(\text{Al1.4|Pt3}))$ where the notation $[X_1:S:X_2]$ corresponds to the thickness sequence between X_1 and X_2 with S being the thickness step. The FTH sample is similar with only a difference in the Pt thickness in the last layers: $\text{Ta5|Pt3|}(\text{Co}[2.0:0.1:2.5]|(\text{Al1.4|Pt3}) (\text{Co}[2.6:0.1:2.0]|(\text{Al1.4|Pt3}))(\text{Co1.0|Al1.4|Pt3}) \times 15|(\text{Co}[2.0:0.1:2.5]|(\text{Al1.4|Pt3}) (\text{Co}[2.6:0.1:2.0]|(\text{Al1.4|Pt2}) (\text{Co2.0|Al1.4|Pt3})$.

The multilayers have been grown on the top side of a Si_3N_4 membrane. For the first (respectively, second) sample, the backside was covered with a 1.1- μm -thick gold mask layer ($\text{Al } 2.5 \text{ nm/Au } 25 \text{ nm}) \times 40$ [respectively, ($\text{Cr } 5 \text{ nm/Au } 55 \text{ nm}) \times 20$] that was milled away with focused ion beam to form a 2- μm (respectively, 800-nm) object hole. For FTH, reference holes of different sizes, typically 30–40 nm, were punched through the whole structure at a distance of 1.8 μm from the object hole center. For HERALDO, the slit used for the reconstructions was 5- μm long and 30-nm wide.

The magnetic hystereses have been measured using AGFM, and SQUID to determine the saturation magnetization at 300 and 80 K.

Magnetic force microscopy and demagnetization. Before imaging, the samples have been demagnetized using an electromagnet, which applied an oscillating magnetic field of exponentially decreasing amplitude. At room temperature, the MFM images have been acquired using cantilevers from TeamNanotech (TN) with nominal stiffness of 3 N/m with its tip capped by 7 nm of magnetic (proprietary) material and 10 nm of Pt. We used a tapping mode with a lift height of 10 nm, at 75% of the drive amplitude with double-passing. The measurements at low temperatures have been performed in a liquid-nitrogen bath with 15 mbars of helium as the exchange gas, using a TeamNanotech tip with a 0-nm lift height and at 50% of the drive amplitude.

FTH reconstruction—Phase Retrieval. The holograms were recorded for left (CL) and right (CR) polarization of the x-ray light in identical conditions at the Co L_3 and then preprocessed for the iterative phase retrieval algorithm. The polarization level of the light is superior to 99%. The left- and right-polarization holograms were first normalized with respect to each other, centered, and any constant offset present was removed. The Fourier transform (FT) of these modified holograms yields a crude real-space image of the cross correlation of the reference holes with the object holes.

The phase retrieval process consists on digitally propagating the reconstructed image back and forth from the reciprocal to the real space, whereas, imposing two constraints. In real space, the support constraint forces the reconstructed image to be located only in the regions where light is actually transmitted (the support is manually constructed using the

FTH reconstructions as a reference), and in reciprocal space, the amplitude of the propagated hologram is forced to match the experimentally recorded one until the algorithm converges to a final reconstruction respecting both constraints. Pixels of the recorded hologram carrying unreliable values (e.g., the pixels shadowed by the beam stop used to protect the camera from the direct beam) were not subjected to the amplitude constraints and their value was left free to change.

Once the data were preprocessed, we began by reconstructing the CL image with a combination of the oversampling smoothness (OSS) algorithm [34] (250 iterations) followed by the solvent flipping (SF) algorithm [26] (200 iterations), which typically yielded a relative error with respect to the experimental hologram of 0.1%. The convergence parameter β started from 0.9 and decreased progressively with an arctan trend down to 0.5 over the OSS iterations. The filter parameter α decreased linearly from the image size down to 0. Then, the solution for CL polarization was used as a starting guess for the CR polarization image, which, thus, only went through the SF algorithm (200 iterations). For each polarization, an average of the 20 reconstructions with the lowest errors was extracted. From that, magnetic contrast is extracted by computing the difference of the two polarized images.

The dark circular background visible in some of the images is an artifact arising from erroneous reconstruction of the missing signal at low frequencies, corresponding to pixels covered by the beam stop for which not only the phase, but also the signal amplitude had to be reconstructed.

HERALDO. Holograms were recorded at the Co L_3 edge for both helicities of the x-ray light. The beam stop is smoothed using the function introduced in Ref. [35]. After normalization and centering, a differential filter was applied to correct one slit, whereas, the other one was set to 0 to cancel the corresponding periodic stripes in the reconstruction. After a Fourier transform of the difference that yields the magnetic

information, the phase of the real-space image is optimized to maximize the contrast, giving the final image. A Gaussian filter with a 0.5 standard deviation was applied to display the final images (not for the analysis).

The image analysis was performed under Matlab using binarization and edge detection to automatically identify isolated objects. Shapes having an aspect ratio bigger than 2.5 and a circularity $C = 4\pi Area/Perimeter^2$ smaller than 0.2 were discarded during the process to eliminate artifacts and elongated stripes. The remaining objects allow to compute the density. Finally, they were fitting using a rotated 2D Gaussian model,

$$z(x, y) = z_0 + A \exp \left[- \left(\frac{(x - x_0) \cos \theta - (y - y_0) \sin \theta}{\sigma_1} \right)^2 - \left(\frac{(x - x_0) \sin \theta + (y - y_0) \cos \theta}{\sigma_2} \right)^2 \right] \quad (1)$$

with x_0 , y_0 , and z_0 as the offsets, A as the amplitude and σ_i as the standard deviations linked to the FWHM with

$$FWHM_i = 2\sqrt{\ln(2)}\sigma_i. \quad (2)$$

Micromagnetic simulations. The micromagnetic simulations were performed using the MUMAX3 solver at zero temperature [28]. To simulate the magnetic state at 300 K, the parameters were fixed as follows: the exchange constant was $A = 18 \text{ pJ m}^{-1}$, the saturation magnetization was $M_S = 1.2 \text{ MA m}^{-1}$, the uniaxial interfacial anisotropy constant was $K_{u,s} = 1.62 \text{ mJ m}^{-2}$, and the interfacial DMI constant was $D_s = 2.34 \text{ pJ m}^{-1}$. Given the complex structure and the variable thickness, each trilayer was divided in three layers, one magnetic, two empty, and the magnetic parameters were diluted depending on the experimental thickness [36]. The total simulation space was made of $512 \times 512 \times 121$ cells, each of size $2 \times 2 \times 1.8 \text{ nm}^3$.

-
- [1] U. K. Röbler, A. N. Bogdanov, and C. Pfeleiderer, Spontaneous skyrmion ground states in magnetic metals, *Nature (London)* **442**, 797 (2006).
- [2] S. Heinze, K. von Bergmann, M. Menzel, J. Brede, A. Kubetzka, R. Wiesendanger, G. Bihlmayer, and S. Blügel, Spontaneous atomic-scale magnetic skyrmion lattice in two dimensions, *Nat. Phys.* **7**, 713 (2011).
- [3] N. Nagaosa and Y. Tokura, Topological properties and dynamics of magnetic skyrmions, *Nat. Nanotechnol.* **8**, 899 (2013).
- [4] A. Fert, N. Reyren, and V. Cros, Magnetic skyrmions: Advances in physics and potential applications, *Nat. Rev. Mater.* **2**, 17031 (2017).
- [5] F. Büttner, I. Lemesch, and G. S. D. Beach, Theory of isolated magnetic skyrmions: From fundamentals to room temperature applications, *Sci. Rep.* **8**, 4464 (2018).
- [6] W. Legrand, J.-Y. Chauleau, D. Maccariello, N. Reyren, S. Collin, K. Bouzehouane, N. Jaouen, V. Cros, and A. Fert, Hybrid chiral domain walls and skyrmions in magnetic multilayers, *Sci. Adv.* **4**, eaat0415 (2018).
- [7] B. Göbel, I. Mertig, and O. A. Tretiakov, Beyond skyrmions: Review and perspectives of alternative magnetic quasiparticles, *Phys. Rep.* **895**, 1 (2021).
- [8] F. N. Rybakov, A. B. Borisov, S. Blügel, and N. S. Kiselev, New spiral state and skyrmion lattice in 3D model of chiral magnets, *New J. Phys.* **18**, 045002 (2016).
- [9] A. Fernández-Pacheco, R. Streubel, O. Fruchart, R. Hertel, P. Fischer, and R. P. Cowburn, Three-dimensional nanomagnetism, *Nat. Commun.* **8**, 15756 (2017).
- [10] D. Raftrey, A. Hierro-Rodriguez, A. Fernandez-Pacheco, and P. Fischer, The road to 3-dim nanomagnetism: Steep curves and architected crosswalks, *J. Magn. Magn. Mater.* **563**, 169899 (2022).
- [11] M. Redies, F. R. Lux, J.-P. Hanke, P. M. Buhl, G. P. Müller, N. S. Kiselev, A. Blügel, and Y. Mokrousov, Distinct magnetotransport and orbital fingerprints of chiral bobbers, *Phys. Rev. B* **99**, 140407(R) (2019).
- [12] F. Zheng, F. N. Rybakov, A. B. Borisov, D. Song, S. Wang, Z.-A. Li, H. Du, N. S. Kiselev, J. Caron, A. Kovács *et al.*, Experimental observation of chiral magnetic bobbers in B20-type fege, *Nat. Nanotechnol.* **13**, 451 (2018).
- [13] A. S. Ahmed, J. Rowland, B. D. Esser, S. R. Dunsiger, D. W. McComb, M. Randeria, and R. K. Kawakami, Chiral bobbers and skyrmions in epitaxial FeGe/Si (111) films, *Phys. Rev. Mater.* **2**, 041401(R) (2018).

- [14] K. Ran, Y. Liu, Y. Guang, D. M. Burn, G. van der Laan, T. Hesjedal, H. Du, G. Yu, and S. Zhang, Creation of a Chiral Bobber Lattice in Helimagnet-Multilayer Heterostructures, *Phys. Rev. Lett.* **126**, 017204 (2021).
- [15] G. P. Müller, F. N. Rybakov, H. Jónsson, S. Blügel, and N. S. Kiselev, Coupled quasimonopoles in chiral magnets, *Phys. Rev. B* **101**, 184405 (2020).
- [16] A. Leonov and K. Inoue, Homogeneous and heterogeneous nucleation of skyrmions in thin layers of cubic helimagnets, *Phys. Rev. B* **98**, 054404 (2018).
- [17] A.-O. Mandru, O. Yildirim, R. Tomasello, P. Heistracher, M. Penedo, A. Giordano, D. Suess, G. Finocchio, and H. J. Hug, Coexistence of distinct skyrmion phases observed in hybrid ferromagnetic/ferrimagnetic multilayers, *Nat. Commun.* **11**, 6365 (2020).
- [18] O. Yildirim, R. Tomasello, Y. Feng, G. Carlotti, S. Tacchi, P. M. Vaghefi, A. Giordano, T. Dutta, G. Finocchio, H. J. Hug, and A.-O. Mandru, Tuning the coexistence regime of incomplete and tubular skyrmions in ferro/ferri/ferromagnetic trilayers, *ACS Appl. Mater. Interfaces* **14**, 29 (2022).
- [19] F. Zheng, F. N. Rybakov, N. S. Kiselev, D. Song, A. Kovács, H. Du, S. Blügel, and R. E. Dunin-Borkowski, Magnetic skyrmion braids, *Nat. Commun.* **12**, 5316 (2021).
- [20] N. Kent, N. Reynolds, D. Raftrey, Ian T. G. Campbell, S. Virasawmy, S. Dhuey, R. V. Chopdekar, A. Hierro-Rodriguez, A. Sorrentino, E. Pereira *et al.*, Creation and observation of hopfions in magnetic multilayer systems, *Nat. Commun.* **12**, 1562 (2021).
- [21] Y. Liu, R. K. Lake, and J. Zang, Binding a hopfion in a chiral magnet nanodisk, *Phys. Rev. B* **98**, 174437 (2018).
- [22] M. Grelier, F. Godel, A. Vecchiola, S. Collin, K. Bouzheouane, A. Fert, V. Cros, and N. Reyren, Three-dimensional skyrmionic cocoons in magnetic multilayers, *Nat. Commun.* **13**, 6843 (2022).
- [23] F. Büttner, B. Pfau, M. Böttcher, M. Schneider, G. Mercurio, C. M. Günther, P. HESSING, C. Klose, A. Wittmann, K. Gerlinger *et al.*, Observation of fluctuation-mediated picosecond nucleation of a topological phase, *Nature Mater.* **20**, 30 (2021).
- [24] M. Guizar-Sicairos and J. R. Fienup, Direct image reconstruction from a fourier intensity pattern using heraldo, *Opt. Lett.* **33**, 2668 (2008).
- [25] S. Eisebitt, J. Lüning, W. F. Schlotter, M. Lörger, O. Hellwig, W. Eberhardt, and J. Stöhr, Lensless imaging of magnetic nanostructures by x-ray spectro-holography, *Nature (London)* **432**, 885 (2004).
- [26] S. Marchesini, A unified evaluation of iterative projection algorithms for phase retrieval, *Rev. Sci. Instrum.* **78**, 011301 (2007).
- [27] H. Popescu, J. Perron, B. Pilette, R. Vacheresse, V. Pinty, R. Gaudemer, M. Sacchi, R. Delaunay, F. Fortuna, K. Medjoubi *et al.*, Comet: A new end-station at soleil for coherent magnetic scattering in transmission, *J. Synchrotron Radiat.* **26**, 280 (2019).
- [28] A. Vansteenkiste, J. Leliaert, M. Dvornik, M. Helsen, F. Garcia-Sanchez, and B. Van Waeyenberge, The design and verification of MuMax3, *AIP Adv.* **4**, 107133 (2014).
- [29] See Supplemental Material at <http://link.aps.org/supplemental/10.1103/PhysRevB.107.L220405> for additional HERALDO reconstructions at remanence and the full hysteresis; magnetotransport measurements at 300 and 80 K and corresponding model used to determine the magnetic anisotropy; the numerical study of the cocoons merging; simulated holography field dependency at both temperatures; the impact of phase retrieval on FTH reconstructions.
- [30] L. Belliard, A. Thiaville, S. Lemerle, A. Lagrange, J. Ferré, and J. Miltat, Investigation of the domain contrast in magnetic force microscopy, *J. Appl. Phys.* **81**, 3849 (1997).
- [31] W. Legrand, D. Maccariello, N. Reyren, K. Garcia, C. Moutafis, C. Moreau-Luchaire, S. Collin, K. Bouzheouane, V. Cros, and A. Fert, Room-temperature current-induced generation and motion of sub-100 nm skyrmions, *Nano Lett.* **17**, 2703 (2017).
- [32] J.-V. Kim and M.-W. Yoo, Current-driven skyrmion dynamics in disordered films, *Appl. Phys. Lett.* **110**, 132404 (2017).
- [33] M. A. Marioni, M. Penedo, M. Bačani, J. Schwenk, and H. J. Hug, Halbach effect at the nanoscale from chiral spin textures, *Nano Lett.* **18**, 2263 (2018).
- [34] J. A. Rodriguez, R. Xu, C.-C. Chen, Y. Zou, and J. Miao, Oversampling smoothness: an effective algorithm for phase retrieval of noisy diffraction intensities, *J. Appl. Crystallogr.* **46**, 312 (2013).
- [35] S. Streit-Nierobisch, D. Stickler, C. Gutt, L.-M. Stadler, H. Stillrich, C. Menk, R. Frömter, C. Tieg, O. Leupold, H. P. Oepen *et al.*, Magnetic soft x-ray holography study of focused ion beam-patterned Co/Pt multilayers, *J. Appl. Phys.* **106**, 083909 (2009).
- [36] I. Lemesh, F. Büttner, and G. S. D. Beach, Accurate model of the stripe domain phase of perpendicularly magnetized multilayers, *Phys. Rev. B* **95**, 174423 (2017).